Available online at www.sciencedirect.com
ScienceDirect
Ceramics International 35 (2009) 2387–2392
CERAMICS INTERNATIONAL
www.elsevier.com/locate/ceramint

Preparation and microstructural characterization of $(Nd_{1-x}Gd_x)_2(Ce_{1-x}Zr_x)_2O_7$ solid solutions

Zhan-Guo Liu, Jia-Hu Ouyang *, Yu Zhou, Xiao-Liang Xia

Institute for Advanced Ceramics, Department of Materials Science, Harbin Institute of Technology, No. 92, West Da-Zhi Street, Harbin 150001, China

Received 27 November 2008; received in revised form 16 December 2008; accepted 2 February 2009
Available online 27 February 2009

Abstract

$(Nd_{1-x}Gd_x)_2(Ce_{1-x}Zr_x)_2O_7$ ($0 \le x \le 1.0$) powders with an average particle size of 100 nm were synthesized with chemical-coprecipitation and calcination method, and were characterized by X-ray diffractometry and scanning electron microscopy. The sintering behaviour of $(Nd_{1-x}Gd_x)_2(Ce_{1-x}Zr_x)_2O_7$ powders was studied by pressureless sintering at 1600–1700 °C for 10 h in air. The relative densities of $(Nd_{1-x}Gd_x)_2(Ce_{1-x}Zr_x)_2O_7$ solid solutions increase with increasing the sintering temperature, and gradually decrease with increasing the content of neodymium and cerium at identical temperature levels. $(Nd_{1-x}Gd_x)_2(Ce_{1-x}Zr_x)_2O_7$ solid solutions have a single phase of defect fluorite-type structure among all the composition combinations studied. The lattice parameters of $(Nd_{1-x}Gd_x)_2(Ce_{1-x}Zr_x)_2O_7$ solid solutions agree well with the Vegard's rule.

Keywords: A. Powders: chemical preparation; A. Sintering; B. Microstructure-final; Ceramics

1. Introduction

In recent years, complex oxides with the general formula of $A_2B_2O_7$ (A = lanthanide, B = Zr, Hf, Ce, Ti, etc.) have been of great interest to many researchers. These compounds exhibit a defect fluorite-type structure or an ordered pyrochlore-type structure, which is mainly governed by the ionic radius ratio of A^{3+} and B^{4+} [1]. They have a wide variety of interesting physical and chemical properties, such as high-melting point, high-thermal expansion coefficient, low-thermal conductivity, high-thermal stability, unique luminescence and high-radiation stability [1]. These properties make them suitable for a variety of applications such as solid electrolytes, catalysts, nuclear waste forms, high-temperature thermal barrier coating materials, etc. [2–8]. New $A_2B_2O_7$-type oxides with varying ionic radius ratios are of considerable scientific interest [9–13]. Nanosized $La_{2-x}Gd_xZr_2O_7$ ($x = 0.025$, 0.05, 0.075 and 0.1) bulk materials synthesized by citrate gel precursor method exhibited a single phase of pyrochlore structure [9]. $Gd_{2-y}La_yZr_2O_7$ ($0 \le y \le 1.0$) solid solutions had a higher oxide-ion conductivity than $Gd_{2-y}La_yZr_2O_7$ ($1.0 < y \le 2.0$) in the temperature range of 200–1000 °C [10,11]. Patwe et al. [12] synthesized $Gd_2Ce_xZr_{2-x}O_7$ ($0 \le x \le 1.0$) ceramics by solid-state reaction method, and found that only 5 mol% of Ce^{4+} is soluble in the lattice of $Gd_2Zr_2O_7$ and there seemed to be no triple phase region in system. Cao et al. [13] prepared $La_2(Zr_{0.7}Ce_{0.3})_2O_7$ by solid-state reaction with their corresponding oxides at 1600 °C, and found that it was a new high-sintering-resistance oxide ceramic material with the structure of mainly fluorite and only a trace of pyrochlore. $(Ln_{1-x}Yb_x)_2Zr_2O_7$ (Ln = Sm, Gd) ($0 \le x \le 1.0$) pressureless-sintered at 1700 °C in air are potential candidates for low-thermal conductivity applications at high temperatures [14,15]. It was reported that morphology and size distribution of nanoparticles had an important influence on materials properties [16]. In the present study, codoped at A sites and B sites of $A_2B_2O_7$, $(Nd_{1-x}Gd_x)_2(Ce_{1-x}Zr_x)_2O_7$ powders were synthesized by chemical-coprecipitation and calcination method. Densification behaviour and microstructure of $(Nd_{1-x}Gd_x)_2(Ce_{1-x}Zr_x)_2O_7$ solid solutions were investigated.

2. Experimental procedure

2.1. Materials preparation

In the present study, neodymium oxide powder (Rare-Chem Hi-Tech Co. Ltd., Huizhou, China; purity ≥99.99%), gadolinium

* Corresponding author. Tel.: +86 451 86414291; fax: +86 451 86414291.
E-mail address: ouyangjh@hit.edu.cn (J.-H. Ouyang).

0272-8842/$36.00
doi:10.1016/j.ceramint.2009.02.009

oxide powder (Rare-Chem Hi-Tech Co. Ltd., Huizhou, China; purity ≥99.99%), cerium nitrate (Rare-Chem Hi-Tech Co. Ltd., Huizhou, China; Analytical) and zirconium oxychloride (Zibo Huantuo Chemical Co. Ltd., China; Analytical) were selected as the reactants. $(Nd_{1-x}Gd_x)_2(Ce_{1-x}Zr_x)_2O_7$ ($x = 0$, 0.1, 0.3, 0.5, 0.7, 0.9, 1.0) powders were synthesized by chemical-coprecipitation and calcination method. Neodymium oxide and gadolinium oxide powders were heat-treated at 900 °C for 2 h in air before weighing as rare-earth oxides were hygroscopic. For each composition, neodymium oxide and gadolinium oxide powders were weighed, and dissolved in dilute nitric acid, while zirconium oxychloride and cerium nitrate were dissolved in distilled water. These solutions were mixed in appropriate proportions and stirred for 60 min at room temperature. The filtered solution was slowly added under stirring to excessive dilute ammonium hydrate solution with a pH value of 12.5 to obtain gel-like precipitates. These gels were washed with distilled water several times to remove Cl^- completely, which was tested by adding the suspension to the $AgNO_3$ aqueous solution, and the absence of precipitation was taken as the proof of the complete removal of Cl^-. The gels were then washed twice in analytically pure alcohol. The remains were dried at 100 °C for 24 h and then calcined at 800 °C for 5 h for crystallization in air. The obtained powders were compacted by cold isostatic pressing at 280 MPa for 5 min. Sintering experiments were carried out in air using the cold-isostatically pressed pellets in a temperature range of 1600–1700 °C at a heating rate of 300 °C h^{-1}. The samples were held for 10 h at sintering temperatures and cooled at a rate of 300 °C h^{-1} down to 800 °C, and then furnace-cooled to room temperature.

2.2. Materials characterization

Crystal structure of synthesized powders was determined by an X-ray diffractometer (Rigaku D/Max-rB, Japan) with Cu Kα radiation at a scan rate of 4°/min. Dilute suspension was taken onto aluminum foil and coated with a thin carbon coating for scanning electron microscope (Hitachi S–4700, Japan) observations. The phases of the sintered samples were characterized by an X-ray diffractometer (Rigaku D/Max 2200VPC, Japan) with Cu Kα radiation at a scan rate of 4°/min. The diffraction peaks of (3 1 1) were also recorded in a step scan mode with a step width of 0.02° and a step time of 3 s. In order to evaluate the lattice parameters, silicon powder was used as the calibration reference. The bulk densities of the cylindrical specimens were estimated from their volumes and masses. The theoretical density of each composition was calculated using lattice parameters acquired from XRD results and the chemical formula weight in an elementary cell. The microstructure of sintered specimens was observed by scanning electron microscope (Hitachi S-4700, Japan). For SEM observations, the specimens were polished with 1 μm diamond paste, and were then thermally etched at 1600 °C for 1 h in air before a thin carbon coating was evaporated onto the surfaces of specimens for electrical conductivity. Qualitative X-ray elemental analysis of specimens was carried out using SEM equipped with energy dispersive spectroscopy (EDS).

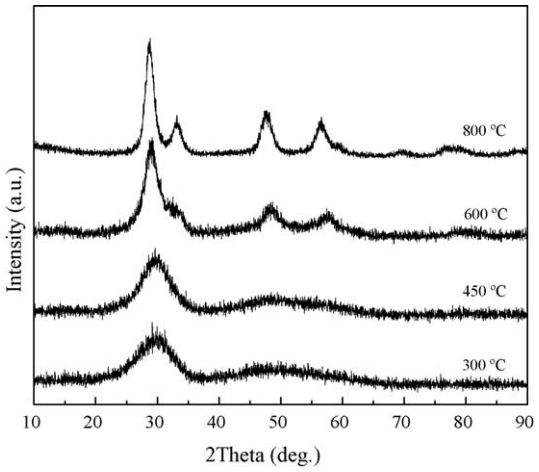

Fig. 1. XRD patterns of $(Nd_{0.5}Gd_{0.5})_2(Ce_{0.5}Zr_{0.5})_2O_7$ powder calcined at different temperatures for 2 h.

3. Results and discussion

Fig. 1 shows the XRD patterns of $(Nd_{0.5}Gd_{0.5})_2(Ce_{0.5}Zr_{0.5})_2O_7$ powder calcined at different temperatures for 2 h in air. It can be seen that $(Nd_{0.5}Gd_{0.5})_2(Ce_{0.5}Zr_{0.5})_2O_7$ powder completely crystallizes at 800 °C within 2 h. The XRD patterns of $(Nd_{1-x}Gd_x)_2(Ce_{1-x}Zr_x)_2O_7$ powders calcined at 800 °C for 5 h in air are shown in Fig. 2. The synthesized powders have wide diffraction peaks and only exhibit a single phase of cubic structure, owing to fine grain sizes of $(Nd_{1-x}Gd_x)_2(Ce_{1-x}Zr_x)_2O_7$ powders. Fig. 3 shows typical morphology of $(Nd_{0.5}Gd_{0.5})_2(Ce_{0.5}Zr_{0.5})_2O_7$ powder. It is clearly that $(Nd_{0.5}Gd_{0.5})_2(Ce_{0.5}Zr_{0.5})_2O_7$ powder has an average particle size of 100 nm in diameter, and exhibits to a certain extent some agglomeration.

The variations in relative density of $(Nd_{1-x}Gd_x)_2(Ce_{1-x}Zr_x)_2O_7$ solid solutions sintered at different temperatures for 10 h are shown in Fig. 4. Clearly, relative densities of all specimens increase with increasing the sintering temperature. With increasing the content of neodymium and cerium in $(Nd_{1-x}Gd_x)_2(Ce_{1-x}Zr_x)_2O_7$ solid solutions, relative density of

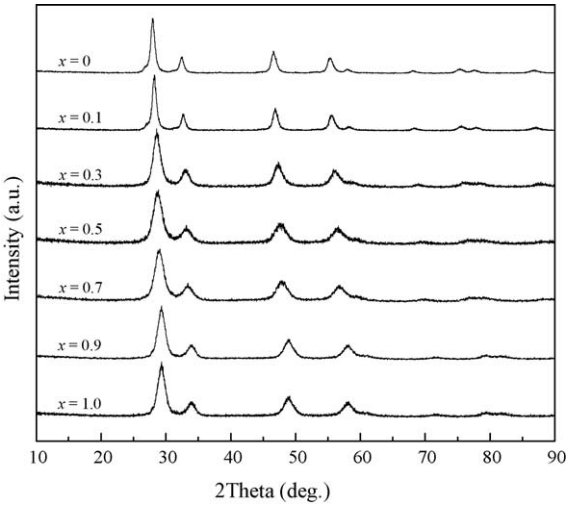

Fig. 2. XRD patterns of $(Nd_{1-x}Gd_x)_2(Ce_{1-x}Zr_x)_2O_7$ powders calcined at 800 °C for 5 h.

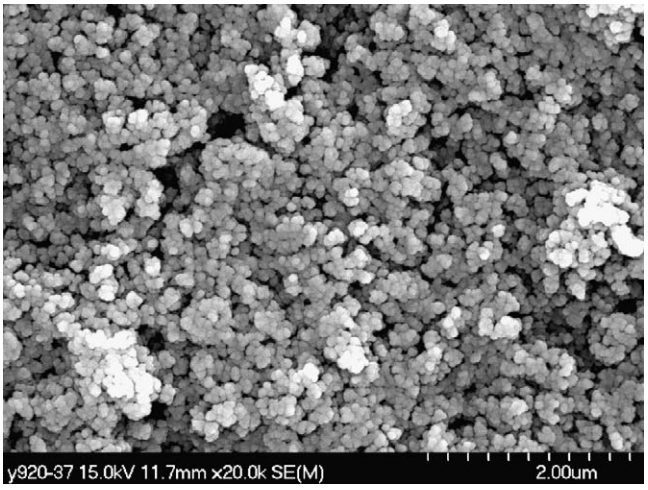

Fig. 3. Morphology of $(Nd_{0.5}Gd_{0.5})_2(Ce_{0.5}Zr_{0.5})_2O_7$ powder calcined at 800 °C for 5 h.

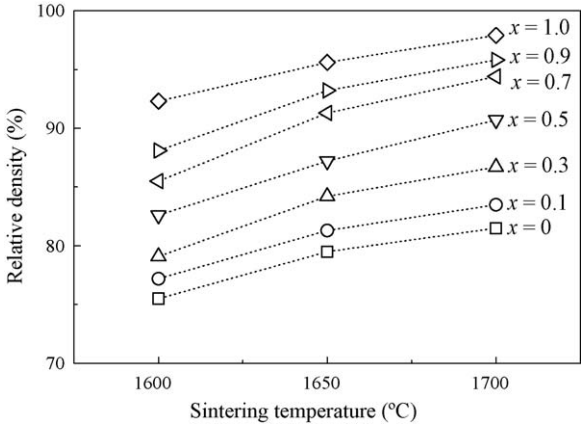

Fig. 4. Variations in relative density of $(Nd_{1-x}Gd_x)_2(Ce_{1-x}Zr_x)_2O_7$ solid solutions with the sintering temperature.

each composition gradually decreases at identical temperature levels.

Fig. 5(a) reveals X-ray diffraction patterns of $(Nd_{1-x}Gd_x)_2(Ce_{1-x}Zr_x)_2O_7$ solid solutions sintered at 1700 °C for 10 h in air. It can be seen that all $(Nd_{1-x}Gd_x)_2(Ce_{1-x}Zr_x)_2O_7$ solid solutions have a single phase of defect fluorite-type structure. The ionic radius of Nd^{3+} and Gd^{3+} are 1.109 and 1.053 Å in the eightfold coordination; however, the ionic radius of Ce^{4+} and Zr^{4+} are 0.87 and 0.72 Å in the sixfold coordination, respectively [17]. The average ionic radius, $r(A_{av.}{}^{3+})$ and $r(B_{av.}{}^{3+})$ of $(Nd_{1-x}Gd_x)_2(Ce_{1-x}Zr_x)_2O_7$ system are estimated from the ionic radius of the component ions and the chemical composition using the following equations:

$$r(A_{av.}{}^{3+}) = x\,r(Gd^{3+}) + (1-x)\,r(Nd^{3+}) \quad (1)$$

$$r(B_{av.}{}^{3+}) = x\,r(Zr^{4+}) + (1-x)\,r(Ce^{4+}) \quad (2)$$

For $(Nd_{1-x}Gd_x)_2(Ce_{1-x}Zr_x)_2O_7$ system, the values of $r(A_{av.}{}^{3+})/r(B_{av.}{}^{3+})$ are in the range of 1.27–1.46, and all compositions exhibit a defect fluorite-type structure, which has

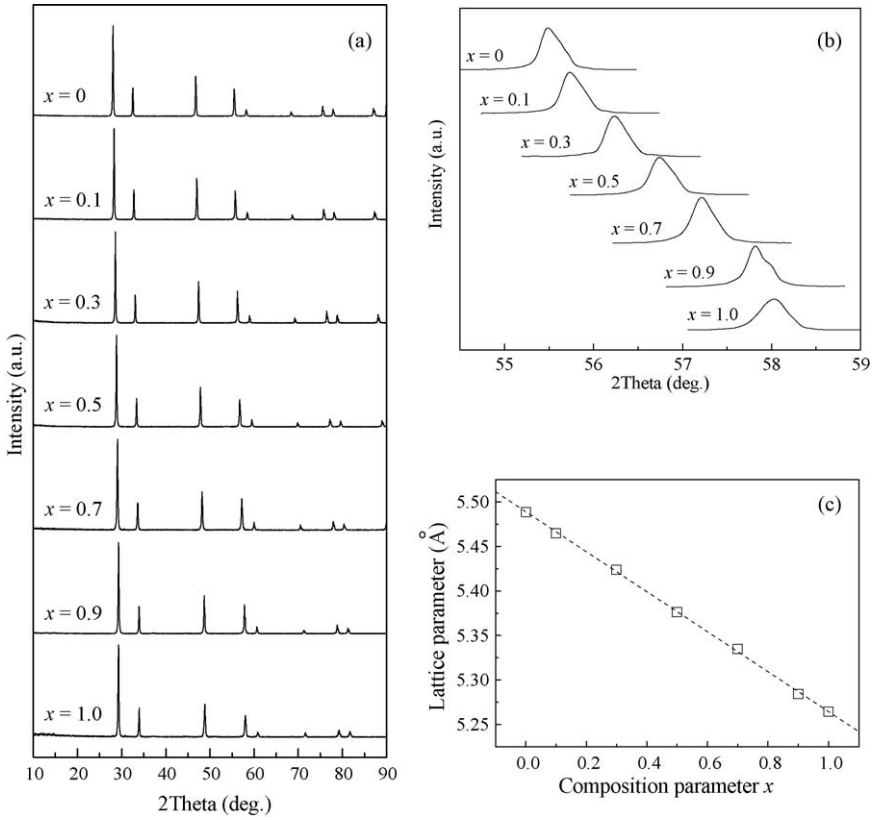

Fig. 5. XRD patterns and derived lattice parameters of $(Nd_{1-x}Gd_x)_2(Ce_{1-x}Zr_x)_2O_7$ solid solutions: (a) 2θ range of 10–90°; (b) a single (3 1 1) peak; (c) lattice parameters derived from (b).

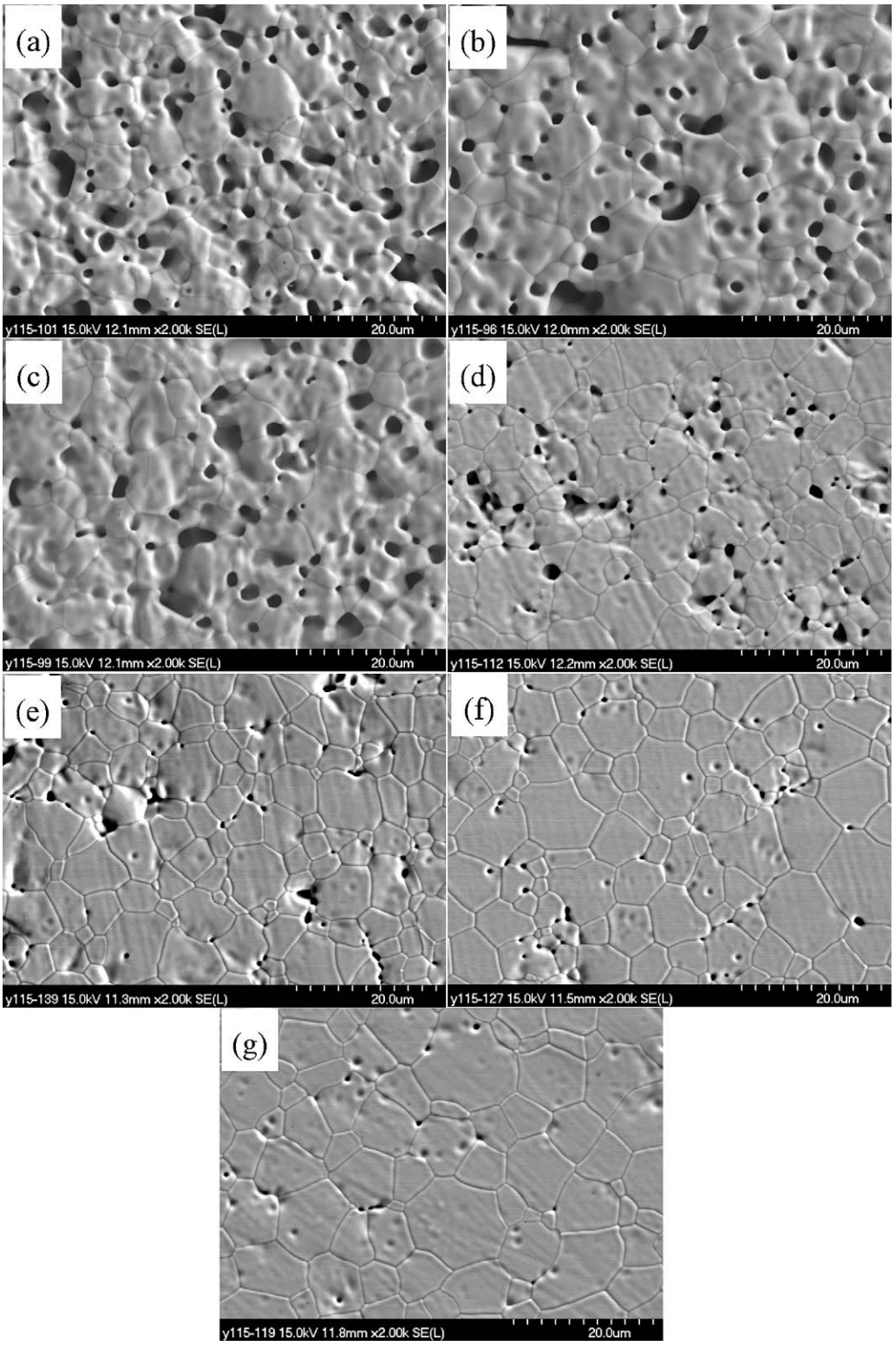

Fig. 6. Microstructures of $(Nd_{1-x}Gd_x)_2(Ce_{1-x}Zr_x)_2O_7$ solid solutions sintered at 1700 °C for 10 h: (a) $x = 0$; (b) $x = 0.1$; (c) $x = 0.3$; (d) $x = 0.5$; (e) $x = 0.7$; (f) $x = 0.9$; (g) $x = 1.0$.

similar rule in the zirconate system. In the zirconate system ($A_2Zr_2O_7$), the stability of pyrochlore structure is limited to the range of $1.46 \leq r(A^{3+})/r(Zr^{4+}) \leq 1.78$ at an atmospheric pressure [1]. Below 1.46, the array of unoccupied anion sites disorders, to produce a defect fluorite structure. Above 1.78, there is a transition to a monoclinic phase with $La_2Ti_2O_7$-type structure. In this case, for $x = 1.0$ ($Gd_2Zr_2O_7$), the $r(A^{3+})/r(B^{4+})$ is equal to 1.46, which resides at the edge of the pyrochlore stability window. It is well known that $Gd_2Zr_2O_7$ undergoes a pyrochlore to fluorite (order–disorder) transition when heated

Table 1
Chemical compositions of $(Nd_{1-x}Gd_x)_2(Ce_{1-x}Zr_x)_2O_7$ solid solutions detected by EDS.

Sintered materials	Mol ratio			
	Nd	Gd	Ce	Zr
$Nd_2Ce_2O_7$	50.5	0	49.5	0
$(Nd_{0.9}Gd_{0.1})_2(Ce_{0.9}Zr_{0.1})_2O_7$	45.8	5.0	44.3	4.9
$(Nd_{0.7}Gd_{0.3})_2(Ce_{0.7}Zr_{0.3})_2O_7$	35.7	15.2	34.3	14.8
$(Nd_{0.5}Gd_{0.5})_2(Ce_{0.5}Zr_{0.5})_2O_7$	25.4	25.3	24.6	24.7
$(Nd_{0.3}Gd_{0.7})_2(Ce_{0.3}Zr_{0.7})_2O_7$	15.3	35.6	14.8	34.3
$(Nd_{0.1}Gd_{0.9})_2(Ce_{0.1}Zr_{0.9})_2O_7$	5.1	45.7	4.9	44.3
$Gd_2Zr_2O_7$	0	49.7	0	50.3

to above 1530 °C [1]. As the sintered temperature used in this work is higher than order–disorder transition temperature, it is not surprising that $Gd_2Zr_2O_7$ exhibits a defect fluorite-type structure in this study. For $(Nd_{1-x}Gd_x)_2(Ce_{1-x}Zr_x)_2O_7$ ($0 \le x \le 0.9$), the $r(A^{3+})/r(B^{4+})$ is clearly less than 1.46, they should have a defect fluorite-type structure. $Nd_2Ce_2O_7$ ceramic synthesized by solid-state reaction with their corresponding oxides at 1600 °C exhibited a defect fluorite-type structure [18], which is coincident with the results in this study.

XRD patterns of $(Nd_{1-x}Gd_x)_2(Ce_{1-x}Zr_x)_2O_7$ solid solutions in a single (3 1 1) peak with a step-scan mode are shown in Fig. 5(b). The (3 1 1) peak that shifts gradually to the high-angle side for $(Nd_{1-x}Gd_x)_2(Ce_{1-x}Zr_x)_2O_7$ when the composition changes from $x = 0$ ($Nd_2Ce_2O_7$) to $x = 1.0$ ($Gd_2Zr_2O_7$). The lattice parameters calculated from these peaks are depicted in Fig. 5(c). An approximately linear decrease of the lattice parameter is observed for $(Nd_{1-x}Gd_x)_2(Ce_{1-x}Zr_x)_2O_7$ system with compositions from $x = 0$ ($Nd_2Ce_2O_7$) to $x = 1.0$ ($Gd_2Zr_2O_7$), which is in a good agreement with the Vegard's rule. This indicates that $Nd_2Ce_2O_7$ and $Gd_2Zr_2O_7$ ceramics are completely soluble.

Fig. 6 shows typical microstructure of $(Nd_{1-x}Gd_x)_2(Ce_{1-x}Zr_x)_2O_7$ solid solutions sintered at 1700 °C for 10 h. It is clearly seen that pores gradually decrease when the composition changes from $x = 0$ ($Nd_2Ce_2O_7$) to $x = 1.0$ ($Gd_2Zr_2O_7$). The average grain size of $(Nd_{1-x}Gd_x)_2(Ce_{1-x}Zr_x)_2O_7$ solid solutions is several micrometers. The chemical compositions of solid solutions were determined by EDS. Table 1 shows the chemical composition analyses of $(Nd_{1-x}Gd_x)_2(Ce_{1-x}Zr_x)_2O_7$ solid solutions. According to the EDS results, the mol ratios of different metallic elements in $(Nd_{1-x}Gd_x)_2(Ce_{1-x}Zr_x)_2O_7$ solid solutions are ±2% different from stoichiometry.

4. Conclusions

$(Nd_{1-x}Gd_x)_2(Ce_{1-x}Zr_x)_2O_7$ oxide powders with an average particle size of 100 nm were synthesized by chemical-coprecipitation and calcination method. The relative densities of $(Nd_{1-x}Gd_x)_2(Ce_{1-x}Zr_x)_2O_7$ solid solutions increase with increasing the sintering temperature, and gradually decrease with increasing the content of neodymium and cerium in $(Nd_{1-x}Gd_x)_2(Ce_{1-x}Zr_x)_2O_7$ at identical temperature levels. $(Nd_{1-x}Gd_x)_2(Ce_{1-x}Zr_x)_2O_7$ solid solutions have a single phase of defect fluorite-type structure among all the composition combinations studied. The lattice parameters of $(Nd_{1-x}Gd_x)_2(Ce_{1-x}Zr_x)_2O_7$ solid solutions agree well with the Vegard's rule. The chemical-coprecipitation and calcination method is an effective technique to mass-produce sinteractive complex oxide powders.

Acknowledgements

The authors would like to thank the financial support from the Program of Excellent Teams in Harbin Institute of Technology (HIT) and the Start-up Program for High-level HIT Faculty Returned from Abroad.

References

[1] M.A. Subramanian, G. Aravamudan, G.V. Subba Rao, Oxide pyrochlores—a review, Prog. Solid State Chem. 15 (2) (1983) 55–143.
[2] K. Shinozaki, M. Miyauchi, K. Kuroda, O. Sakurai, N. Mizutani, M. Kato, Oxygen-ion conduction in the $Sm_2Zr_2O_7$ pyrochlore phase, J. Am. Ceram. Soc. 62 (9–10) (1979) 538–539.
[3] J.M. Sohn, M.R. Kim, S.I. Woo, The catalytic activity and surface characterization of $Ln_2B_2O_7$ (Ln = Sm, Eu, Gd and Tb; B = Ti or Zr) with pyrochlore structure as novel CH_4 combustion catalyst, Catal. Today 83 (1–4) (2003) 289–297.
[4] S. Lutique, D. Staicu, R.J.M. Konings, V.V. Rondinella, J. Somers, T. Wiss, Zirconate pyrochlore as a transmutation target: thermal behaviour and radiation resistance against fission fragment impact, J. Nucl. Mater. 319 (2003) 59–64.
[5] R. Vassen, X.Q. Cao, F. Tietz, D. Basu, D. Stőver, Zirconate as new materials for thermal barrier coatings, J. Am. Ceram. Soc. 83 (8) (2000) 2023–2028.
[6] M. Peters, C. Leyens, U. Schulz, W.A. Kaysser, EB-PVD thermal barrier coatings for aeroengines and gas turbines, Adv. Eng. Mater. 3 (4) (2001) 193–204.
[7] Z.-G. Liu, J.-H. Ouyang, Y. Zhou, Preparation and thermophysical properties of $(Nd_xGd_{1-x})_2Zr_2O_7$ ceramics, J. Mater. Sci. 43 (10) (2008) 3596–3603.
[8] Z.-G. Liu, J.-H. Ouyang, Y. Zhou, Structural evolution and thermophysical properties of $(Sm_xGd_{1-x})_2Zr_2O_7$ ($0 \le x \le 1.0$) ceramics, J. Alloys Compd. 472 (2009) 311–316.
[9] K. Koteswara Rao, N. Anantharamulu, M. Salagram, M. Vithal, Preparation, characterization and ESR studies of bulk and nano sized pyrochlore $La_{2-x}Gd_xZr_2O_7$ ($x = 0.025$, 0.05, 0.075 and 0.1), Spectrochim. Acta A 66 (3) (2007) 646–649.
[10] J.A. Díaz-Guillén, M.R. Díaz-Guillén, J.M. Almanza, A.F. Fuentes, J. Santamaría, C. León, Effect of La substitution for Gd in the ionic conductivity and oxygen dynamics of fluorite-type $Gd_2Zr_2O_7$, J. Phys.: Condens. Matter 19 (35) (2007) 356212.
[11] J.A. Díaz-Guillén, M.R. Díaz-Guillén, K.P. Padmasree, A.F. Fuentes, J. Santamaría, C. León, High ionic conductivity in the pyrochlore-type $Gd_{2-y}La_yZr_2O_7$ solid solution ($0 \le y \le 1$), Solid State Ion. 179 (38) (2008) 2160–2164.
[12] S.J. Patwe, B.R. Ambekar, A.K. Tyagi, Synthesis, characterization and lattice thermal expansion of some compounds in the system $Gd_2Ce_xZr_{2-x}O_7$, J. Alloys Compd. 389 (1–2) (2005) 243–246.
[13] X. Cao, J. Li, X. Zhong, J. Zhang, Y. Zhang, R. Vassen, D. Stőver, $La_2(Zr_{0.7}Ce_{0.3})_2O_7$—a new oxide ceramic material with high sintering-resistance, Mater. Lett. 62 (17–18) (2008) 2667–2669.
[14] Z.-G. Liu, J.-H. Ouyang, Y. Zhou, J. Li, X.-L. Xia, Influence of ytterbium- and samarium-oxides codoping on structure and thermal conductivity of zirconate ceramics, J. Eur. Ceram. Soc. 29 (4) (2009) 647–652.
[15] Z.-G. Liu, J.-H. Ouyang, Y. Zhou, J. Li, X.-L. Xia, Densification, structure, and thermophysical properties of ytterbium–gadolinium zirconate

ceramics, Int. J. Appl. Ceram. Technol., 2008, doi:10.1111/j.1744-7402.2008.02289.x.

[16] R. Chaim, M. Levin, A. Shlayer, C. Estournes, Sintering and densification of nanocrystalline ceramic oxide powders: a review, Adv. Appl. Ceram. 107 (3) (2008) 159–169.

[17] G.S. Rohrer, Structure and Bonding in Crystalline Materials, Cambridge University Press, Cambridge, 2004, pp. 521–525.

[18] H. Dai, X. Zhong, J. Li, J. Meng, X. Cao, Neodymium–cerium oxide as new thermal barrier coating material, Surf. Coat. Technol. 201 (6) (2006) 2527–2533.